Polymer Bulletin (2022) 79:6141–6172
https://doi.org/10.1007/s00289-021-03795-7

ORIGINAL PAPER

Development of functional chitosan-based superabsorbent hydrogel nanocomposites for adsorptive removal of Basic Red 46 textile dye

Hafida Ferfera-Harrar[1] · Tayeb Benhalima[1,2] · Amina Sadi[1]

Received: 18 March 2021 / Revised: 28 May 2021 / Accepted: 21 June 2021 /
Published online: 28 June 2021

Abstract

Hydrogel nanocomposites comprised of chitosan-grafted-hydrolyzed polyacrylamide as matrix and montmorillonite clay as nanofiller CTS-g-PAAm/MMT were synthesized in aqueous phase by using Triton X-100 surfactant as porogen agent with the aim to apply as adsorbents for the removal of Basic Red 46 (BR46) dye. The as-prepared ampholytic hydrogels, denoted as M/MMTx ($x = 0$, 2, 5, and 10 wt.% of clay loading), were characterized by X-ray diffraction, scanning electron microscopy, thermogravimetric analysis, and Fourier transform infrared spectroscopy. The nanohybrid hydrogels exhibited mostly exfoliated structure of the MMT layers and presented morphology that is more porous as compared to the virgin matrix. Also, the thermal stability was marginally affected by clay loading. Study on the swelling behavior showed remarkable water super-absorbing ability, salt-, and pH-sensitivity. The adsorption performances were evaluated by varying clay content, adsorbent dose, pH, initial dye concentration, contact time, and temperature. The results showed that the sorption rates were fast and more than 78% of adsorption capacities were achieved within nearly 30 min using 0.1 g L^{-1} sorbent dose in 200 mg L^{-1} of dye solution. The nonlinear kinetics and isotherm adsorption models fitted on the experimental data correlated well with pseudo-second-order kinetics and Langmuir models. Also, the intra-particle diffusion mechanism is not rate-limiting step and the adsorption was suggested to occur mainly via electrostatic interactions and hydrogen bonding. The maximum Langmuir adsorption capacities (q_m) of the matrix and the optimized nanocomposite M/MMT2 were found to be 1553 and 1813 mg g^{-1}, respectively. Thermodynamic parameters revealed that sorption process was endothermic and spontaneous. Moreover, effective regeneration was obtained in four adsorption–desorption cycles and about 92% of the adsorbed dye was released from hydrogels. Results obtained from this study suggest that the prepared hydrogel nanocomposites could be promising adsorbents for removing cationic dyes from polluted water.

Extended author information available on the last page of the article

Keywords Hydrogel nanocomposites · Chitosan · Clay · Dye adsorption · Reusability

Introduction

Environmental issues are among the main challenges of the twenty-first century. The continuous discharging of effluents from the industrial processes produced by industries, such as textiles, leather, cosmetics, paper, plastics and rubber, has led to the spread of toxic and carcinogenic compounds in the aquatic environment, influencing human health and ecological equilibrium.

Synthetic dyes are among important types of water pollutants considering their large-scale production, usage and toxic/mutagenic nature causing harmful effects on living organisms and serious water pollution concerns [1, 2].

Basic Red 46 (BR46) is a synthetic basic dye that is widely used in textile, paper and printing industries. Like other synthetic dyes, BR46 is also discharged into the surface waters, imparting red color, both during its manufacture and from dyeing industries [3]. Human exposure to BR46 dye may cause dermatitis, skin irritation, and provoke harmful health effects to the fauna.

Many treatment technologies have been employed to removing dyes from wastewater, such as chemical precipitation, ion exchange, coagulation, membrane separation, catalytic degradation, adsorption [4–8]. Adsorption has been regarded as the most promising and considered more accessible as an economical and effective method for removing various types of pollutants owing to its admirable features such as low cost, easy-handling operation, insensitivity to toxic substances, and high efficiency and availability of various adsorbents [7, 8].

Despite its extensive use in water and wastewater treatment industries, activated carbon remains an expensive absorbent. The need for safe and economical methods for the elimination of pollutants from contaminated waters has compelled research interest toward eco-friendly and low-cost adsorbents as alternatives to commercially available activated carbon [9, 10].

Various adsorbents have been used for the removal of pollutants from contaminated waters, including clay, zeolites, agricultural, and industrial waste by-products [11–14]. As well, natural polymers from biological or vegetable resources have been regarded as a good tool to minimize the environmental impact. Among them, polysaccharide-based materials such as cellulose and its derivatives, chitosan, alginate, carrageenan have been extensively applied as adsorbents owing to distinctive advantages as availability, renewability, biodegradability cost-effectiveness, and safety. Particularly, chemical modifications on the polysaccharides could be made via functionalization, grafting, etc., to improve their property profile for a broad spectrum of end-uses. Moreover, polysaccharides have a capacity to associate by physical and chemical interactions with various molecules owing to the presence of functional groups, which is convenient to eliminate a wide ranging of toxic pollutants such as dyes and heavy metal ions through attractive interactions, chelating, and coagulating/flocculating [15–17]. Hence, adsorption on polysaccharide derivatives can be a cost-efficient technique of choice in water

decontamination for extraction and separation of compounds, and a useful tool for protecting the environment.

In this regard, sustainable hydrogels based on polysaccharides have engrossed much interest in different applications such as wastewater treatment, soil conditions, and drug delivery [18–20]. Compared with traditional adsorbents, hydrogels have gain particular concern in water purification owing to their ease of preparation, effectiveness, regeneration abilities, and reuse. In addition, the structure of hydrogel could be flexibly designed, and their properties could be adjusted by altering the type and number of functional groups according to usage requirement. Likewise, during the hydrogels synthesis, graft copolymerization of appropriate monomers onto polysaccharides backbone leads to improve their mechanical and physicochemical properties and customizes them to respond to external stimuli such as temperature and pH and so meet the requirements of both easy-to-handle and expectable adsorption performances in wastewater treatment [21–23].

Montmorillonite (MMT), principal layered silicate component of bentonite, is nontoxic, low-cost and widely available in Algeria. MMT has received considerable attention as promising adsorbents for the removal of organic dyes and heavy metals owing to its several exceptional properties such as large specific surface area, high hydrophilicity, biocompatibility, low toxicity, high cationic exchange capacity [24, 25]. Despite this, the difficulty of separating MMT particles from wastewater after adsorption process limits their individual use. The approach of clay encapsulation into hydrogels networks has been widely adopted to allow their exceptional features to be combined, such as elasticity and permeability of hydrogels with the high capacity of clay to adsorb several substances and to overcome their distinct drawbacks. In this way, interest on preparation of polysaccharide/clay hydrogel nanohybrids adsorbents has grown exponentially to improve or provide new properties to the original material [26–28].

Chitosan (CTS) is a polysaccharide derived from chitin made up with two different monomers N-acetylglucosamine and glucosamine linked through β-(1 → 4)-glycosidic bonds. It has been widely used alone or combined (natural/synthetic polymers blends, hybrid organic–inorganic composites) for several applications. In particular, the presence of functional amino and hydroxyl groups makes CTS a potential adsorbent for heavy metal and cationic/anionic dyes due to its chelating ability. In addition, grafting copolymerization of hydrophilic monomers via these reactive groups has allowed improving the adsorptive CTS performances [29–32].

In earlier research work, we have reported on the synthesis and the properties studies of smart superabsorbent hydrogel nanocomposites made of natural/synthetic polymers as matrix, namely chitosan-graft-poly(acrylamide), and MMT clay as nano-reinforcing [33]. The study was focused on the influence of clay loading into the matrix on morphology, thermal stability, and water absorbency. It was also reported that the partial hydrolysis of the amide groups of PAAm chains at high pH significantly improved their swelling properties in various media. All these properties make them attractive for environmental applications as eco-friendly adsorbents to trap heavy metals and dyes from contaminated water. In addition, these hydrogels have presented antibacterial activity against bacteria *(Staphylococcus aureus* and

Escherichia coli) that may be an alternative to conventional disinfection processes in wastewater treatment intended for reuse.

On the other hand, the porosity of hydrogels plays a prominent role in enhancing their aptitude for water uptake and pollutants sorption. An effective method frequently used for preparing porous hydrogels is by introducing surfactants pores generator and then extracted with a suitable solvents [34–36]. Indeed, surfactants can self-assemble to form micelles in aqueous environment, which act as templating porogen in the gelling process.

Herein, we extend the previous study to synthesize and characterize hydrolyzed hydrogel nanocomposites chitosan-graft-poly(acrylamide)/MMT via free-radical aqueous polymerization by adding Triton X-100 surfactant as pore-forming template. The water absorbency and swelling kinetic were investigated. Following this step, we explore their adsorptive ability for the removal of Basic Red 46 (BR46) dye as pollutant model. Several sorption-affecting factors, such as clay loading, solution pH, adsorbent dose, dye concentration, contact time, and temperature, were examined. Isotherms, kinetics, thermodynamic parameters, and modeling of adsorption process as well as reusability of adsorbents were studied. To our best knowledge, study of BR46 adsorption onto polysaccharide-based hydrogels nanomaterials has not yet been reported in literature.

Experimental

Materials

Chitosan (CTS) with 75% degree of deacetylation, medium average molecular weight, and viscosity 200–800 cps was purchased from Prochima Sigma-Aldrich (Tlemcen, Algeria). Acrylamide (AAm), potassium persulfate (KPS), *N,N*-methylene-bisacrylamide (MBA) of analytical grade and Triton X-100 (T) of laboratory grade were purchased from Sigma-Aldrich Chemical Co (St Louis, USA). All chemicals, sodium chloride (NaCl) and ethanol, were of analytical grade and used as received from Sigma-Aldrich Chemical Co (St Louis, USA). Doubly distilled water (DDW) was used in all the experiments. Montmorillonite (MMT) clay with size fraction (<2 µm) was extracted from bentonite category of Maghnia Roussel that was kindly supplied by ENOF Chemical Research Company (Algiers, Algerian). The MMT was homoionized with sodium cations, and its cationic exchange capacity (CEC) about 86.16 mequiv/100 g was previously determined by conductometrie [37]. The Basic Red 46 dye (BR46) was purchased from the Alfaditex textile manufacturing company (Algiers, Algerian).

Preparation of the hydrogel adsorbents

A series of hydrolyzed hydrogel nanocomposites were produced through aqueous radical graft copolymerization and crosslinking of AAm monomer onto CTS backbone in presence of MMT clay at various contents (2, 5, and 10 wt% with

respect to AAm) using potassium persulfate as initiator and *N,N*'-methylene-bisacrylamide as crosslinker by following the earlier reported procedure with minor changes [33]. First, required amount (1 g) of CTS was dissolved in 30 mL 1% (v/v) acetic acid solution in three-neck flask; then, certain amount (0.4 wt. %) of Triton X-100 was added into the chitosan solution and stirred vigorously for 30 min to form the foamed chitosan. After being purged with nitrogen, the flask was placed in bath at 60 °C for 10 min, and then KPS (2 wt.%) was added to the mixture under stirring for 15 min to generate radicals. Separately, the clay was dispersed in the solution and ultrasonicated for 30 min and added to solution of AAm (5 g) and MBA (1 wt%). After stirring for 15 min and sonication for 10 min, the suspension was introduced into the funnel kept under nitrogen flux and then added to the reactional flask for 2 h. Afterward, the resulting gel was washed thoroughly with DDW, followed by solution mixture of ethanol/water (8:1, v/v) for several times to remove the surfactant. Subsequently, the hydrogel was cut into small pieces and subjected to hydrolysis treatment in 1 N NaOH solution at 95 °C during 2 h and the pH of the gel solution was adjusted to 6.0 by adding 1.0 M of acetic acid solution. The product was washed excessively with DDW and then dehydrated in excess of ethanol for 24 h. Next, it was dried in oven at 60 °C, ground to particles size of 40–60 mesh, and stored for later use.

The MMT-free hydrogel matrix CTS-graft-PAAm was also prepared using the above procedure, as reference. The free MMT matrix hydrogel and its nanocomposites are denoted as M/MMT**x**, where $\boldsymbol{x} = 0, 2, 5, 10$ wt% of clay content.

Characterization

X-ray diffraction (XRD) patterns of pristine MMT and hydrolyzed hydrogels were collected on a Bruker D8 advance diffractometer (Bruker, Germany) by employing CuKα radiation (40 kV, $\lambda = 1.5406$ A^0) in 2θ range 1–30° with 0.01°/s scan rate.

The surface morphology of the hydrogels was observed by a scanning electron microscopy (SEM), JSM-6360LV Scanning Electron Microscope (JEOL, USA) using an acceleration voltage of 10 kV. The samples were sputter-coated with a thin layer of gold prior analysis.

Thermal stability of hydrogels was investigated by Thermogravimetric analysis (TGA) on Q500 analyzer, (TA instruments, USA). Samples (2–2.5 mg) were heated in alumina crucible from 30 to 600 °C at 10 °C/min under nitrogen flow (50 ml/min).

Fourier transform infrared spectroscopy (FTIR) spectra of samples prepared using KBr pellets were recorded on a Vector 33 FTIR spectrometer (Bruker, Germany) in 4000–400 cm^{-1} range at a resolution of 2 cm^{-1}. FTIR and SEM (FEI & Nova NanoSEM450) operating at an accelerating voltage of 15 kV were used for free- and dye-loaded hydrogels in order to identify the structural and morphological changes after dye adsorption onto free- and dye-loaded hydrogels.

Swelling measurements

Swelling behavior of the hydrolyzed hydrogels was studied at room temperature in DD water, saline solution (0.9 wt. %), and pH solutions. Triplicate tests were carried out, and average values were reported in this study. The procedure is as follows: a pre-weighted hydrogel sample (0.05 g) was soaked in the selected medium (400 mL) and allowed to reach equilibrium. After that, the swollen sample was filtrated through an 80-mesh stainless steel screen, drained for 30 min, and then weighed. The swelling capacity at equilibrium (S_{eq}) (g/g) was evaluated by using Eq. (1). Kinetics of swelling was also studied by pouring the pre-weighted samples (0.05 g) in excessive DD water and taken out at desired time intervals. The swollen samples were weighted after wiping off the excessive water by gently tapping the surfaces with wet filter. This procedure was repeated until there was no further weight increase. The swelling capacity at any time (S_t) was calculated according to Eq. (1), in where (S_{eq}) is expressed as (S_t) [33].

pH-sensitivity of these hydrogels was also examined. The pH solutions ranging from 2 to 11 were made from stock 1 N HCl and 1 N NaOH and adjusted using a pH-meter (DELTA-320).

$$S_{eq}\ (g/g) = \frac{W_s - W_d}{W_d} \tag{1}$$

where W_d and W_s are the sample's weights in the dry and the swollen states, respectively.

Adsorption experiments

Batch adsorption experiments of BR46 dye onto the grafted matrix and its nanocomposites were carried out at controlled temperature in pH media under stirring at 200 rpm using an orbital shaker. Typically, a required amount (m) of each adsorbent was mixed with a volume (V) of dye aqueous solution at initial concentration (C_0), and then the mixture was shaken until reaching equilibrium. The concentration of the residual dye in solution was evaluated by analyzing the filtered supernatant using UV–Vis spectrophotometer (Specord 200, Analytic Jena, Germany) at 530 nm and using previously made calibration curves from stock dye solutions of 1000 mg L^{-1}. All tests were conducted in triplicate, and mean values were considered for the fitting process.

The adsorption capacity at equilibrium (q_e, mg g^{-1}) and the related removal efficiency R (%) were calculated using Eqs. (2) and (3), respectively [35, 36].

$$q_e = \frac{C_0 - C_e}{m} \times V \tag{2}$$

$$R\ (\%) = \frac{C_0 - C_e}{C_0} \times 100 \tag{3}$$

where C_0 and C_e (mg L^{-1}) are dye concentrations at initial and equilibrium times, respectively. V (L) is the volume of dye solution, and m is the weight of adsorbent (g).

The MMT content effect on adsorption performances of the grafted hydrogels was studied for fixed C_0 of 200 mg L^{-1} and 0.1 g L^{-1} of sorbent at pH 7 for 3 h of contact time.

The effect of solutions pH ranging from 4 to 10 was studied in dye solution of C_0 200 mg L^{-1} using 0.1 g L^{-1} of adsorbent dose at 25 °C for 3 h. The pH values were adjusted using 0.1 N NaOH or 0.1 N HCl and were assessed by pH-meter DELTA-320 (accuracy ± 0.1).

The effect of varying hydrogels mass from 0.025 to 0.2 g L^{-1} on dye adsorption was carried out in dye solution of $C_0 = 50$ mg L^{-1} at pH 7 for 3 h of contact time.

The temperature effect was investigated in the range of 25–45 °C using 0.1 g L^{-1} of adsorbent dose in dye solution of C_0 equal to 200 mg L^{-1} for 3 h in neutral pH.

All the adsorption experiments were performed in triplicate with the mean taken.

Adsorption kinetic studies were performed at 25 °C ± 0.2 by adding 0.1 g L^{-1} of adsorbent dose in dye solution of $C_0 = 200$ mg L^{-1}. The different adsorbent-dye solutions were shaken and then withdrawn at desired intervals until reaching equilibrium states. The amount of adsorbed dye at any time (q_t) was calculated according to Eq. (1), where (q_e, C_e) are expressed as (q_t, C_t).

Isotherm adsorption experiments were conducted by varying the dye initial concentration C_0 in the range of 50–800 mg L^{-1} and by adding 0.1 g L^{-1} of adsorbent dose in neutral pH for 3 h. The values of q_e and R (%) were determined using Eq. (1) and (2), respectively.

Regeneration and reusability experiments

The reuse of adsorbents is required to make adsorption process economical and suitable at commercial scale. Therefore, the reusability of MMT-free hydrogel and its typical nanocomposite were explored for four adsorption/desorption cycles conferring to our previously works [35, 36]. Adsorption tests were conducted in dye solution of 200 mg L^{-1} using 0.1 g L^{-1} of samples at 25 °C for 3 h. For desorption study, the dye-loaded samples were rinsed from the adsorption medium and immersed in NaCl solution 0.5 M of water/ethanol mixture (50/50 v/v), used as desorbing solvent, at 25 °C under gentle shaking (50 rpm) for 3 h. After washing with DDW, the regenerated samples were reused for succeeding cycles. The percentage of dye desorbed from adsorbents was determined using Eqs. (4) and (5) [16, 36].

$$\text{Desorption } (\%) = \frac{q_{des}}{q_{ads}} \times 100 \tag{4}$$

$$q_{des} = \frac{C_{des}\ V}{m} \tag{5}$$

where q_{des}, C_{des}, V, and m represent the amount of the desorbed dye, dye concentration in desorbing solution, volume of solution, and hydrogel sample weight, respectively.

Results and discussion

Structure and morphological characterization of the hydrogel nanocomposites

Figure 1 illustrates the formation of the hydrolyzed hydrogel nanocomposites. As we reported earlier, the persulfate ions ($S_2O_8^{2-}$) decompose thermally to anionic sulfate radicals ($SO4^{\bullet-}$), which generate active radicals sites onto CTS chains [33]. Afterward, these CTS–$O^{\bullet}$ macro-radicals intercalate into MMT layers to increase their inter-layers spacing and then initiate grafting and copolymerization of the adsorbed AAm molecules into inter-foliar and on layer surfaces. Then, the chains crosslinking in the presence of different amounts of encapsulated MMT particles led to the formation of grafted network nanocomposites.

As shown in Fig. 1, during the subsequent hydrolysis with NaOH solution, the amide sides groups of PAAm chains converted partially to carboxylate ions (COO^-) with degree of hydrolysis of about 60% and the release of ammonia. The formed anionic PAAm, which is a copolymer of acrylamide and acrylic acid sodium salt (COO^-Na^+), could improve the functional performance of the obtained materials. Simultaneously, some crosslinking reactions of CTS chains during alkaline hydrolysis have also been highlighted.

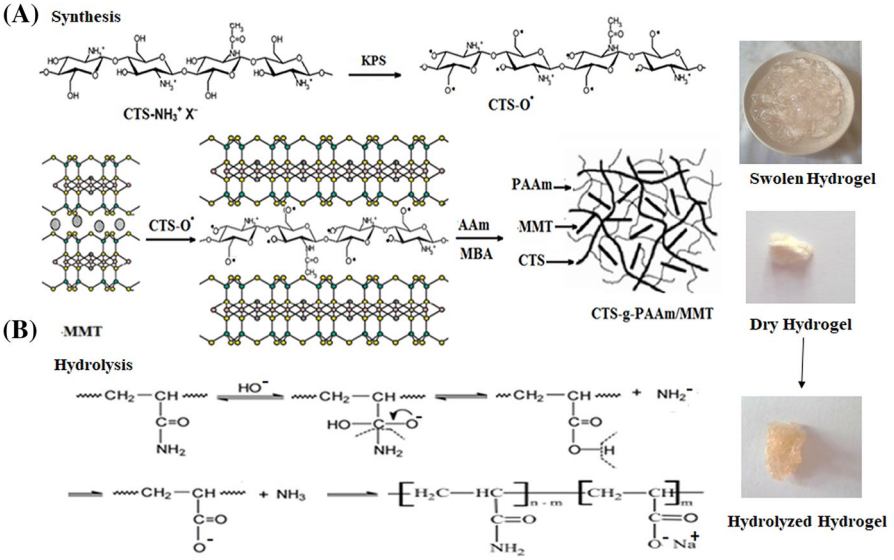

Fig. 1 Schematic illustration of the synthesis and hydrolysis of the hydrogel nanocomposites and the photographs of the obtained hydrogels

Thus, the hydrolysis treatment generates grafted network as matrix comprised of several functional groups, namely amide ($COONH_2$), amine (NH_2), hydroxyl (OH), and carboxylate (COO^-) anions, resulting in hydrogel with ampholytic properties and adsorptive ability.

It is interesting to mention that the presence of the unconverted $–CONH_2$ groups could act as chelating sites for binding metal ions and cationic dyes as well as via ion–dipole interactions by the carbonyl C=O groups and by hydrogen bonding. Then, the chitosan-grafted-hydrolyzed PAAm hydrogel, which present ability to associate with molecules via physical and chemical interactions, is promising material to be applied as versatile adsorbent in the removal of both cationic and anionic dyes from the simulated wastewater.

XRD analysis is commonly conducted to ascertain the intercalated or exfoliated structure of nanocomposites. XRD diffractograms of pristine MMT, hydrolyzed hydrogel nanocomposites, and their virgin matrix (M/MMT**x**, $x = 0$, 2, 5, 10) are presented in Fig. 2a. The MMT clay exhibits the typical diffraction peak in the low-angle region at $2\theta = 6.76°$ ($d_{001} = 1.30$ nm) that disappears when MMT is incorporated in all nanohybrids, suggesting that MMT platelets are mostly exfoliated into nanocomposites structure. This result is in agreement with previous studies reported on hydrogel nanocomposites based on chitosan-*g*-poly(acrylic acid) and MMT [38] or organo-rectorite [39]. Indeed, it is well known that chitosan is polycationic in acidic media. This polyelectrolyte behavior happens as the amino groups ($-NH_2$) on the surface of chitosan protonate to cationic amine groups ($-NH_3^+$). As can be seen from Fig. 1, in acidic solutions, the CTS chains rich in $-NH_3^+$ groups display an extended structure that may facilitate their intercalation into layers of MMT through cation-exchange process [40]. Accordingly, the protonated CTS could first intercalate into interlayers spaces of MMT layers via electrostatic interactions between the $-NH_3^+$ groups and the negatively charges of clay layer surfaces by exchanging Na^+ cations. Subsequently, the CTS-intercalated MMT undergoes in situ graft copolymerization with AAm to form the nano-hybrid. During polymerization reaction, both growth and crosslinking of the confined PAAm chains expend MMT inter-layers space and provoke the exfoliation of layers, which is evidence by no detection of the typical diffraction peak of the stacked MMT layers in the XRD profiles of the nanocomposites.

It is also noted that exfoliated structure has also been highlighted for the unhydrolyzed hydrogel nanocomposites counterparts [33], indicating that hydrolysis treatment and the use of Triton X-100 surfactant did not influence the dispersion level of the clay platelets within nano-hybrid networks.

SEM micrographs of the elaborated hydrogels are shown in Fig. 2b. The grafted matrix displays loose and coarse surface with some pores and gaps. For nanocomposites, particularly for 2 and 5 wt.% of MMT contents, an increase in surface roughness and many apparent microspores are observed, but their diameters are uneven. Also, no separation of organic/inorganic phases is noticed, indicating the homogeneity of the hydrogels as real composites, in agreement with XRD findings. This affinity may be promoted by hydrogen interactions between the matrix groups and the clay hydroxyls [33]. On the other hand, the surfaces of these hydrogels appear more porous as compared to those of the counterparts

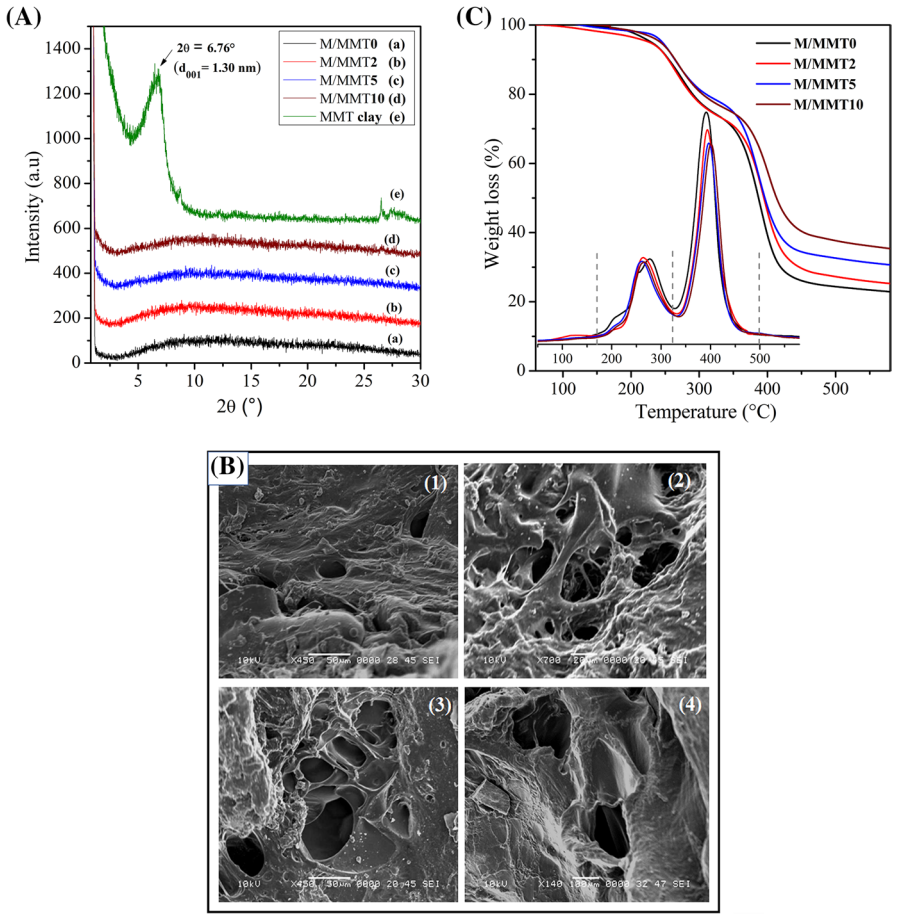

Fig. 2 **a** XRD patterns of MMT, hydrolyzed matrix hydrogel and its nanocomposites; **b** SEM micrographs of the elaborated hydrogels in the presence of surfactant: (1) matrix M/MMT**0**, (2) M/MMT**2**, (3) M/MMT**5**, (4) M/MMT**10**; **c** TGA and d(TG) thermograms of the hydrogels

previously prepared in absence of the Triton X-100 [33]. This morphological change can be assigned to the effect of the added surfactant. Indeed, prior to crosslinking, the self-assembly of the surfactant molecules generates spherical micelles in chitosan solution that acts as template for pores forming and endows the network additional spaces, which are convenient for the penetration of water molecules and then contribute to improve the swelling properties. Hence, the addition of MMT at low loading (less than 5 wt.%) and surfactant have great influence on the surfaces porosity of the hydrogel nanocomposites.

Thermal stability study

The thermal stability of the hydrogels was assessed by TGA. Figure 2c shows TGA and d (TG) thermograms of free MMT matrix and its nanocomposites. The grafted matrix displays three thermal decomposition stages. The minor initial weight loss up to 160 °C less than 2 wt% is due to adsorbed and bound water moisture. The second weight loss about 22 wt% in the range of 160–326 °C may be attributed to the elimination of NH_2 of carboxamide groups in PAAm as ammonia, MBA crosslinker, and hydroxyl groups of CTS as H_2O molecules. The third stage, which starts at about 328 °C and extends to 500 °C, with about 54% weight loss shows a temperature of maximum degradation T_{max} at 392 °C. This main substantial mass loss is due to complex chain scissions of PAAm and of CTS compound through the dehydration of saccharide rings and breaking of C–O–C glycosidic bonds and thus the destruction of the grafted network structure [41, 42]. The hydrogel nano-hybrids curves display similar degradation behavior to the MMT-free hydrogel; however, a slight enhance in thermal stability is noticed. The influence of the incorporated MMT is evidenced in the main degradation by shifting of both temperatures of onset and maximal degradation T_{onset} and T_{max} of matrix up to, respectively, 335 °C and 400 °C with increasing MMT content to 10 wt.%. Furthermore, the weight losses up to 585 °C observed for MMT-loaded hydrogels are lower than free matrix, and also the residue values increase from 22.9% for matrix to 24.14%, 30.67%, and 35.06% by adding 2, 5, and 10 wt.% of MMT, respectively. This result suggests that MMT acts as retarding agent of degradation process owing to its higher thermal stability than the polymeric chains as well as to the 'tortuous path' effect of clay layers that delay the permeation of oxygen and the escape of volatile degradation products [33].

Swelling properties

For environmental application of hydrogels as adsorbents of metal ions and dyes pollutants of wastewater, it is important to study their dynamic swelling, which is greatly influenced by their structure porosity and hydrophilic functional groups.

Figure 3a, b illustrates the swelling kinetic in DDW for all hydrogels and their absorbency values in water and saline 0.9 wt.% NaCl solution. Overall, the absorption capacities sharply increase within the earlier 10 min and then began to level off until reaching the equilibrium state.

This increase in water absorbency is owed to the presence of hydrophilic groups of anionic PAAm ($–CONH_2$, $–COO^-$) and CTS ($–NH_2$, –OH) compounds of the grafted matrix. In addition, the mutual electrostatic repulsions between the carboxylate ions, known for their high hydrophilicity, induce PAAm chains expansion and hence an increase in water absorbency.

Even though the hydrogel nanohybrids exhibit similar swelling tendency as compared to virgin matrix, it is noticed higher initial swelling rates and the corresponding equilibrium swelling ratios increase with increasing MMT content until 5 wt. %, beyond which a decrease in absorbency is observed. Previous studies [38, 42, 43] have reported comparable effect of inorganic additives like MMT, attapulgite,

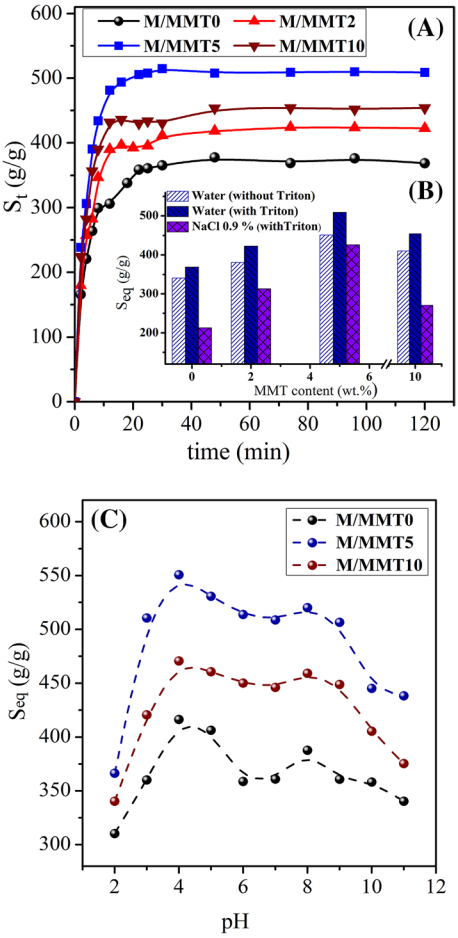

Fig. 3 **a** Swelling kinetic of hydrolyzed matrix hydrogel and its nanocomposites in DD water, **b** absorbency values in DD water and 0.9% saline solution and **c** swelling behavior in various pH media

and muscovite clays on swelling performance of chitosan-g-poly(acrylic acid) based hydrogel nanocomposites. This enhance in affinity for water uptake with an increase of MMT from 0 to 5 wt % can be explained by the fact that –OH groups on the surface of MMT layers could react with the functional groups of matrix through hydrogen bondings and provide extra crosslinking points, which could improve the network structure, and thus enhance water absorbency. Also, more mobile cations of MMT (principally Na^+) are present in the matrix that contributes to increase osmotic pressure difference between the network and the external solution, and thus enhances hydrophilicity of corresponding nanocomposite for a greater absorption.

Further increasing MMT content to 10 wt% results in a decrease of swelling ability. Indeed, the presence of lot of –OH groups on the surface of MMT generates more chemical and physical cross-linkages into network that decreases polymer chains elasticity and prevents effective anion–anion electrostatic repulsions of PAAm chains, leading to lower water absorbency.

It is noteworthy that the swelling capacities of these hydrogels synthesized by using Triton X-100 are greater than the counterparts ones obtained earlier in absence of surfactant [33]. For instance, the absorbency of nanocomposite containing 5 wt.% of MMT increases from 450 to 508 g g^{-1} by introducing pore-forming agent Triton X-100. Similarly, Wei [34] has reported on the study of starch-g-poly(acrylic acid) superabsorbents that the content of Triton X-100 has greatly improved their water absorbency and swelling rate. The author has found that the porous sample prepared with surfactant (0.4%) needed only 5 min to reach 80% of its equilibrium as compared to the nonporous one (90 min) [34]. Also, as previously pointed out [35, 36], the use of sodium n-dodecyl sulfate (SDS) surfactant during the gelation of CMC-based hydrogels has promoted faster subsequent water uptake than those prepared in absence of SDS.

Besides, all hydrogels display swelling tendency in saline solution similar to that in DDW but with lower absorbency values. This swelling loss is ascribed to the charge screening effect generated by Na^+ cations in the swelling medium, which shields the COO^- anions and reduces the anion–anion electrostatic repulsions. As a result, the osmotic pressure between the network and the external solution decreases, and the absorbed water is driven out of network.

The swelling pH-sensitivity of nanocomposites and virgin matrix is also examined (Fig. 3c) displays. As the pH of medium increases, the water uptake of both hydrogels increases with a same trend where two maxima are detected at around pH 4 and 8. Indeed, in acidic media $pH \leq 4$, the swelling capacity is promoted by the dominant charges NH_3^+ since the carboxylate COO^- ions become protonated to COOH groups. Conversely, in media of $6 < pH < 10$, the prevalent ionized forms of COO^- ions develop mutual electrostatic repulsions that augment osmotic pressure inside network, thereby giving rise to upper swelling capacity.

Study of BR46 dye adsorption onto hydrogel nanocomposites

Effect of MMT content

Figure 4a displays the evolution of equilibrium adsorption capacity (q_e) and the removal efficiency R (%) as function of MMT loading into hydrogels. Upon increasing MMT content, the values of q_e and R (%) are gradually increased from 931 mg g^{-1} and 84.27% for native hydrogel to reach an optimum of 1026.2 mg g^{-1} and 87.45% for M/MMT**2** nanohybrid. It is also noticed that the effectiveness of dye removal R (%) from solution onto adsorbent is marginally affected by only 3%, while the related adsorptive capacity q_e is improved by about 95 mg $^{g\text{-}1}$. In agreement with SEM deductions, this result could be attributed mainly to a more porous morphology observed for MMT-incorporated hydrogel, which results in greater specific surface area of adsorbent, which can be defined as the portion of the total surface area that is available for adsorption. This fact promotes the entrapped dye molecules onto the surface to diffuse inside network and their retention by inner active sites. Accordingly, the amount of adsorbed dye (mg) per unit mass of adsorbent is perceptibly augmented. Likewise, the greater affinity of

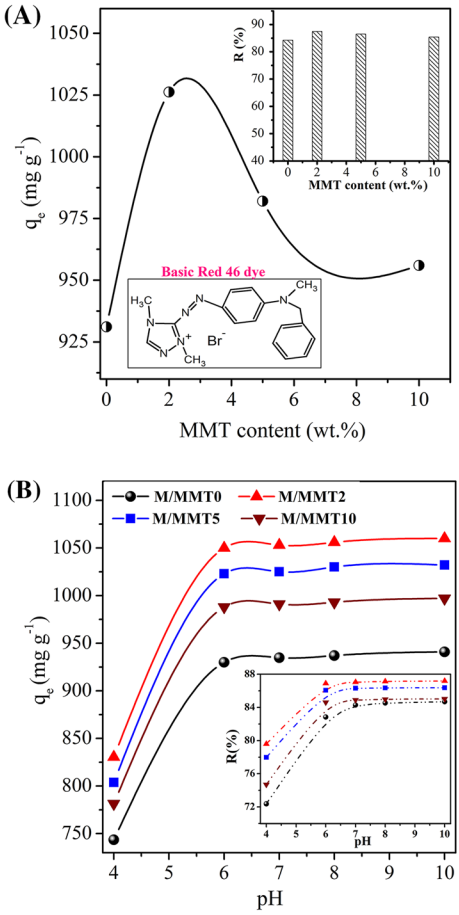

Fig. 4 Effects of **a** MMT content, **b** solution pH on adsorption of dye onto hydrogel matrix and its nanocomposites (inset: removal efficiency R (%) and structure of Basic Red 46 dye ($C_0 = 200$ mg L^{-1}, adsorbent dose = 0.1 g L^{-1}, pH 7, 25 °C, 3 h)

hydrogel nanocomposites for BR46 dye as compared to virgin hydrogel is due to convenience of more active binding sites availability of the added MMT, which possesses outstanding adsorptive ability for various pollutants. Indeed, the BR46 dye molecules may be adsorbed onto nanohybrids through electrostatic interactions between its cationic-N + group and negatively charged surface of MMT layers as well as by hydrogen bonding that occurs between the nitrogen-containing groups of dye and the OH groups of MMT. However, beyond the clay content of 2 wt. %, the adsorption values (q_e and R (%) diminish slightly but remain higher than those of native matrix. This fact may be interpreted by two reasons: (i) MMT particles occupy increasingly interstitial spaces and pores within network, resulting in reduced available spaces, (ii) at higher MMT content, extra crosslinking points are generated into the network via hydrogen bonding between OH groups of clay and those of matrix compounds (CTS and hydrolyzed PAAm). As a result, the elasticity of network decreases and leads to less penetration of water/dye molecules.

Analogous adsorptive behavior for cationic dyes was confirmed onto hydrogel nanocomposites k-carrageenan/poly(vinyl alcohol)/MMT [43], carboxymethyl cellulose/k-carrageenan/activated MMT [44], chitosan-g-poly(acrylic acid)/MMT [45], chitosan-g-poly(acrylic acid)/attapulgite [46], and chitosan-g-poly(acrylic acid)/vermiculite [47]. Herein, the hydrogel nanocomposite M/MMT**2** is selected as typical adsorbent to further understand the adsorption process.

Effect of solution pH

The initial pH of dye solution is an important controlling factor in adsorption process since it may affect the adsorbent surface charge and so the affinity for dye pollutant. Figure 4b shows the influence of pH on the evolution of adsorption capacity at equilibrium q_e (mg g^{-1}) of the grafted hydrogel M/MMT**0** and its M/MMT**x** nanohybrids over the pH range of 4–10. Overall, hydrogels show almost the same trend for the adsorption change in various pH solutions, regardless of clay loading, indicating that the added MMT has no influence on pH dependence of adsorption. As it can be seen, the qe values increase sharply with rising pH from 4 to 6 and, thereafter, gradually with further increase in pH until 10. Indeed, in acidic pH media (pH < 6), this behavior is belonging to the protonation of the amino –NH2 groups of CTS, resulting in repulsive electrostatic interactions with the positive charges of dye molecules. Additionally, at lower pH solution, hydrogen ions compete with dye cation, and most of the carboxylate ions of adsorbent exist in carboxylic form of –COOH, which reduce the adsorbed amounts for RB46 dye molecules [48–50]. Beyond pH 6 and in alkaline media the ionized $COO-$ groups are generated and thus enhance the electrostatic attraction affinity toward the cationic dye.

As expected, the uppermost adsorption values (q_e, R%) are attained onto M/MMT**2**, whatever the initial pH of dye solution. These values are arranged in increasing order for dye sorption onto nanohybrids and matrix as M/MMT2 > M/MMT5 > M/MMT10 > M/MMT0. Accordingly, for example at pH4, the values of (q_e, R %) decrease as (830, 79.6%) > (804, 77.9%) > (781.5, 74.7%) > 743.6, 72.3%) for MMT content ***x*** of 2, 5, 10 wt.% and onto virgin matrix, respectively. However, in basic medium at pH8 these values become upper and arranged as (1056, 87.2%) > (1030, 86.3%) > (993, 84.5%) > (937, 84.5%). Similar behavior has been observed in adsorption studies of MB dye onto chitosan-g-poly(acrylic acid)/clay [45–47]. All other adsorption factors were studied in neutral dye solution.

Effect of adsorbent dose and influence of temperature

Figure 5a displays the effect of adsorbent dose on adsorption capacity and removal efficiency for BR46 dye. Regardless of MMT content, it is clear that all hydrogels M/MMT**x** exhibit comparable adsorptive behavior, where the adsorption capacity decreases consistently by increasing adsorbent mass from 0.025 to 0.2 g L^{-1}. Concurrently, R (%) values increase speedily with increasing dose up to 0.1 g L^{-1}, beyond which no significant changes are obtained. For instance, the adsorption values of q_e and (R%) onto M/MMT**2** nanocomposite, which exhibits the uppermost adsorption data, diminish from 1644 mg g^{-1} (82.2%) to

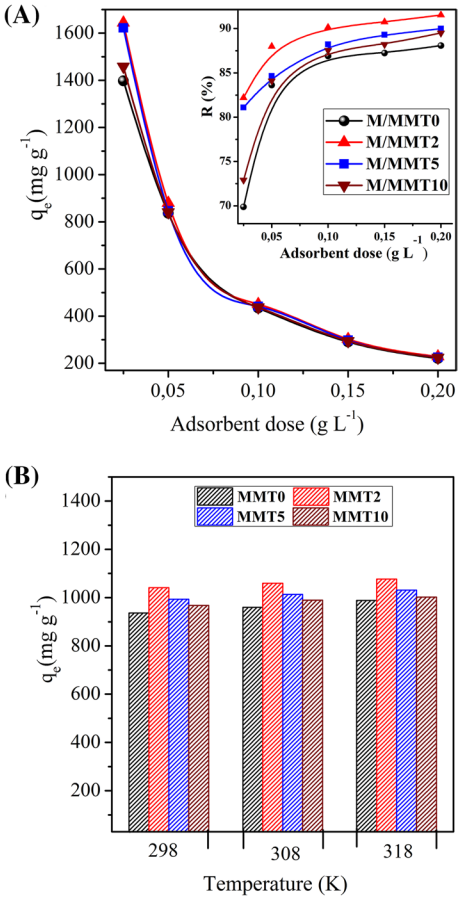

Fig. 5 Effects of **a** adsorbent dose (inset: removal efficiencies *R* (%)) and **b** temperature on dye adsorption capacities onto the grafted hydrogel matrix and its nanocomposites (experimental conditions: pH 7, 3 h of contact time ((**a**): $C_0 = 50$ mg L^{-1}, 25 °C), ((**b**): $C_0 = 200$ mg L^{-1}, sorbent dose = 0.1 g L^{-1})

450.65 mg g^{-1} (90.13%) by increasing adsorbent amount from 0.025 to 0.1 g L^{-1}. These findings support that adsorbent shows maximum adsorption capacity at lower adsorbent doses. Indeed, as the mass of adsorbent increases, the active sites on the adsorbent become increasingly overlapped. This behavior leads to lower surface area, and so the quantity of adsorbed dye per gram adsorbent decreases. Beyond a dose of 0.15 g L^{-1}, the active sites for dye binding become not available due to aggregation formation of the adsorbent particles, and so the adsorption did not change. These observations agreed with earlier studies on removal of cationic dyes using carboxymethyl cellulose- [36, 37, 51] and alginate-based composites hydrogels [52, 53].

The influence of temperature on BR46 dye adsorption onto matrix and its nanocomposites was studied at 298, 308, and 318 K. As shown in Fig. 5b, all adsorbents exhibit a slight increase in their sorption capacity by raising the temperature, suggesting an endothermic process nature. Hence, all subsequent experiments were conducted at 25 °C.

Effect of contact time

Considering the adsorption rate as a crucial parameter for practical applications, the influence of contact time effect on adsorption was examined using the elaborated hydrogels and the obtained results are shown in Fig. 6a. Initially, the adsorption capacity increases rapidly up to 30 min, where almost 78% of dye molecules get adsorbed. Afterward, it slows down until 60 min, beyond which there is no significant increase. Initially, the adsorption capacity increases sharply owing to the abundant availability of active sites on adsorbents surfaces. Later, upon gradual occupancy of these sites, adsorption becomes sluggish with the passage of time until reaching steady state, indicating equilibrium.

It can be also observed that the amount of the dye adsorbed on nanocomposite hydrogels is greater than that adsorbed on M/MMT**0** matrix. For instance, the values of q_e and $R(\%)$ values reach 1026 mg g^{-1} and 87.45% for M/MMT**2** after time contact of 160 min, while those of MMT-free hydrogel were found to be 931 mg g^{-1} and 84.27%, respectively. Photographs in Fig. 6b showing dye solutions before and after adsorption together with the tested samples confirm the adsorptive performance of hydrogels. Hence, the time required to achieve the equilibrium sorption of the dye being about 60 min for all hydrogels.

Effect of initial dye concentration

The effect of initial concentration C_0 of dye solutions on equilibrium adsorption capacity (q_e) and removal R (%) was assessed, and the results are presented in Fig. 7. As it can be seen, the q_e values increase sharply as C_0 increases from 50 to 800 mg

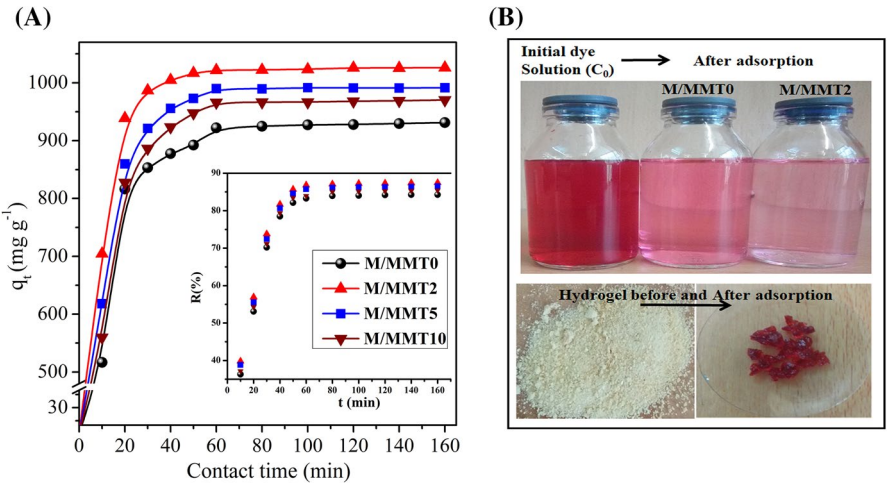

Fig. 6 **a** Effect of contact time on BR46 dye adsorption using hydrogel matrix and its nanocomposites (inset: removal efficiency for BR46 dye) (C_0 of 200 mg L^{-1}, adsorbent dose of 0.1 g L^{-1}, pH7, at 25 °C); **b** photographs of dye solutions and hydrogels samples before and after adsorption tests (C_0 = 200 mg L^{-1}, 0.1 g L^{-1} of adsorbent, 1 h)

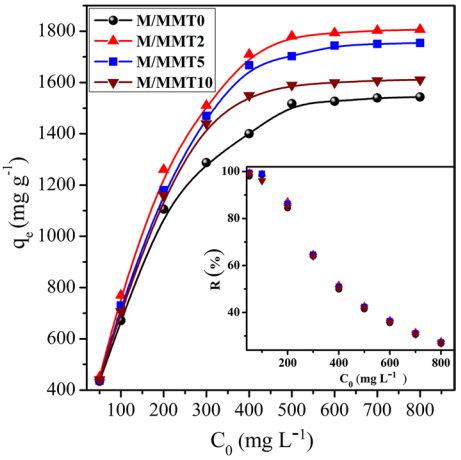

Fig. 7 Effect of dye initial concentration on adsorption capacity and removal efficiency using hydrogel matrix and its nanocomposites (C_0 from 50 to 800 mg L^{-1} at 0.1 g L^{-1}, pH 7, 25 °C, 3 h of contact time)

L^{-1} followed by slight rise until reaching maximum sorption around 300 mg L^{-1} for all sorbents. Oppositely, the efficiency of removal decreases with increasing C_0. This behavior can be correlated with the reason of driving forces caused by pressure gradient, which is originated from concentration rising. Indeed, at low concentration, the ratio of dye to the huge number of available binding sites is low, which favor adsorptive removal of BR46 dye molecules. Thereafter, for C_0 more than 300 mg L^{-1}, the majority of active sites are saturated and thus their ability to retain more dye molecules decreases, so irrelevant adsorption is discerned. Additionally, dye molecules undergo aggregation in upper C_0, which delay their diffusion into adsorbent particles.

Likewise, polysaccharide-based composites adsorbents, comprising carboxymethyl cellulose, alginate, chitosan, κ-carrageenan, agar, etc., exhibited maximum sequestration of dyes at higher initial dye concentration [36, 37, 43–45, 51–53].

As expected, the presence of the entrapped MMT particles into the hydrogel matrix favors dye molecules absorbing. Indeed the porous structure of the hydrogel nanocomposites improves the contact opportunities between these adsorbents and dye, via mainly electrostatic interactions of carboxylate (COO^-) as well as the negatively charges of clay layers with the cationic dye. The hydroxyls groups of clay may also contribute to attach dye through hydrogen bonding. The maximum equilibrium adsorption capacities (q_e,exp) are found to increase from 1543 mg g^{-1} for matrix to 1806, 1754, and 1610 mg g^{-1} by adding MMT into the matrix at 2, 5, and 10 wt.%, respectively, while the related removal efficiency (%) remains close.

Characterization of dye-loaded hydrogel adsorbents

The FTIR spectra of M/MMT**0** hydrogel and its typical nanocomposite M/MMT**2** before and after dye adsorption given in Fig. 8a are recorded to ascertain the presence of dye molecules into the dye-loaded hydrogel and potential chemical interactions.

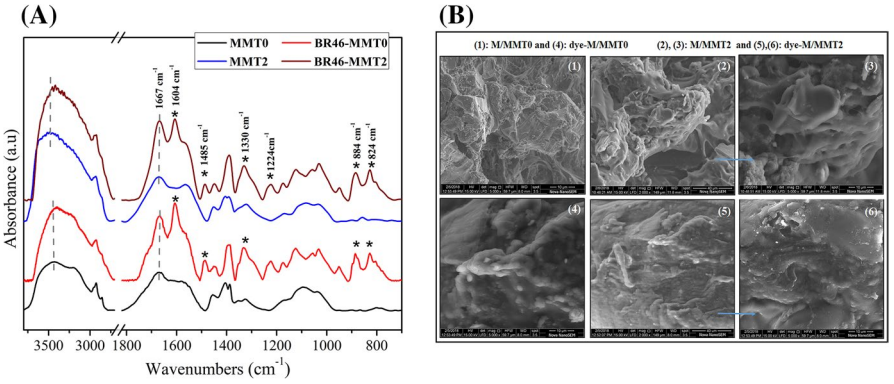

Fig. 8 **a** FTIR spectra and **b** SEM micrographs at high magnifications (2000×, 5000×) of matrix hydrogel M/MMT**0** and its M/MMT**2** nanocomposite before and after adsorption

By comparing spectra of dye-loaded adsorbents to their unload counterparts, additional bands characteristics of BR46 dye appear after adsorption. Principally, it is noticed the bands at 884 and 824 cm^{-1} ascribed to out-of-plane bending vibrations of =C–H of heterocycle and aromatic ring, at 1224 cm^{-1} due to C–N stretching of aliphatic amine, and at 1485 cm^{-1} due to N=N stretching that overlaps N–H bonding vibrations. The sharply intensified peak at 1330 is assigned to stretching vibrations of C–N aromatic amine bonds. As well, the perceptible peaks at 1667 and 1604 cm^{-1} are due to stretching vibrations of C=N (as well $C=N^+$ bonds) and of C=C in aromatic ring of dye molecules, which overlap the bands of the grafted CTS-g-PAAm network, namely stretching C=O vibrations of acetyl groups (amide I) and of asymmetric $\nu_{C=O}$ of carboxylate groups. It can be deemed that COO^- ions act as active sites in adsorption process through electrostatic interactions with $C=N^+$ groups of the cationic dye [37, 51–54].

Apart from this, the broad band due to stretching vibrations of N–H (ν_{N-H}) from amide and amino groups as well as O–H groups (ν_{O-H}, symmetric) of the network shifts remarkably after adsorption from 3442 to 3397 cm^{-1} for matrix and from 3486 to 3417 cm^{-1} for its nanocomposite. This behavior suggests the participation of these functional groups of the grafted matrix (as well hydroxyls groups of the MMT clay in the case of nanocomposite) in the adsorption process via hydrogen bonding interactions with N-containing groups of the dye [54]. From these results, it is suggested that the adsorption of dye onto hydrogel adsorbents takes place through the formation of hydrogen bonding and ionic interactions.

On the other hand, SEM micrographs of unload and dye-loaded nanocomposite M/MMT**2**, recorded at different magnifications to confirm the morphological surfaces changes, are given in Fig. 8b. As it can be seen, the nanocomposite present rough and porous surface, but after adsorption of dye the surface becomes smooth and visibly unlike. Indeed, the cavities seem to be covered by dye molecules, and more relaxed structure with a paste-like texture is perceived. This prominent alteration of surfaces highlights the effectiveness of BR46 dye adsorption onto nanocomposite adsorbent. According to our previous SEM findings [33], these CTS-PAAm/

MMT**x** hydrogel nanocomposites demonstrated more loose porous and rough structures surfaces than MMT-free matrix. This porous morphology helps water to act as a transport channel for dye molecules and thus promote their bonding to active sites on the surface and inside cavities of the grafted network.

Adsorption kinetic models

The adsorption kinetics was investigated for understanding mechanism of sorption process. The frequently applied pseudo-first-order (PFO) and pseudo-second-order (PSO) kinetic models were utilized to simulate the experimental data [55–57] as well as the intra-particle diffusion model proposed by Weber and Morris to explain the diffusion mechanism involved in adsorption [58].

Nonlinear forms of PFO and PSO kinetic expressions are shown in Eq. (6) and Eq. (7), respectively.

$$q_t = q_{e1}\left(1 - e^{-k_1 t}\right) \tag{6}$$

$$q_t = \frac{k_2 q_{e2}^2 t}{\left(1 + q_{e2} k_2 t\right)} \tag{7}$$

where q_e and q_t (mg g^{-1}) are the amounts of the adsorbed BR46 at equilibrium and at time t (min), respectively.

k_1 (min^{-1}) and k_2 (g mg^{-1} min^{-1}) are the adsorption rate constants of pseudo-first-order and pseudo-second-order models, respectively. The parameters including k_1, k_2, and q_e are calculated by fitting q_t versus t of the above equations using MATLAB 2013 program.

Determining the best-fitting model is a key analysis to mathematically describe the involved sorption system and, therefore, to explore the related theoretical assumptions. Hence, several error calculation functions have been widely used to estimate the error deviations between experimentally and theoretically predicted equilibrium adsorption values [16]. In this study, two statistical functions have been used to investigate their applicability as suitable tools to evaluate kinetic and isotherm models fitness, namely the correlation coefficient of determination (R^2) and the sum of square error (SSE) [59, 60] according to Eqs. (8) and (9), respectively.

$$R^2 = \frac{\left(q_{i,\ exp} - \bar{q}_{i,\ cal}\right)^2}{\sum_{i=1}^{n}\left(q_{i,exp} - \bar{q}_{i,cal}\right)^2 + \left(q_{i,exp} - q_{i,cal}\right)^2} \tag{8}$$

$$SSE = \sum_{i=1}^{n}\left(q_{i,exp} - q_{i,cal}\right)^2 \tag{9}$$

where $q_{i,exp}$ and $q_{i,cal}$ are the experimental and the calculated amount of the adsorbed BR46 dye.

From error analysis, if the data from a model are similar to the experimental data, SSE will be a small number and conversely if they strongly differ.

The nonlinear kinetic model plots are presented in Fig. 9, and the adsorption parameters, the correlation coefficients R^2, and the error analysis (SSE) are given in Table 1.

Figure 9 shows obviously that the pseudo-second-order model is most suitable for modeling the adsorption of BR46 onto hydrogel matrix and its nanocomposites. From Table 1, for all adsorbents, the R^2 values of pseudo-second-order model ($R^2 \geq 0.998$) are slightly greater than of pseudo-first-order model and the calculated values (q_{e2}) obtained from the pseudo-second-order model are close to the experimental data (q_e,exp). Moreover, the error function SSE for dye sorption onto matrix and nanocomposites is arranged as pseudo-first-order $^{>>}$ pseudo-second-order, which reveals the fitness of pseudo-second-order kinetics model to the dye adsorption data onto hydrogels.

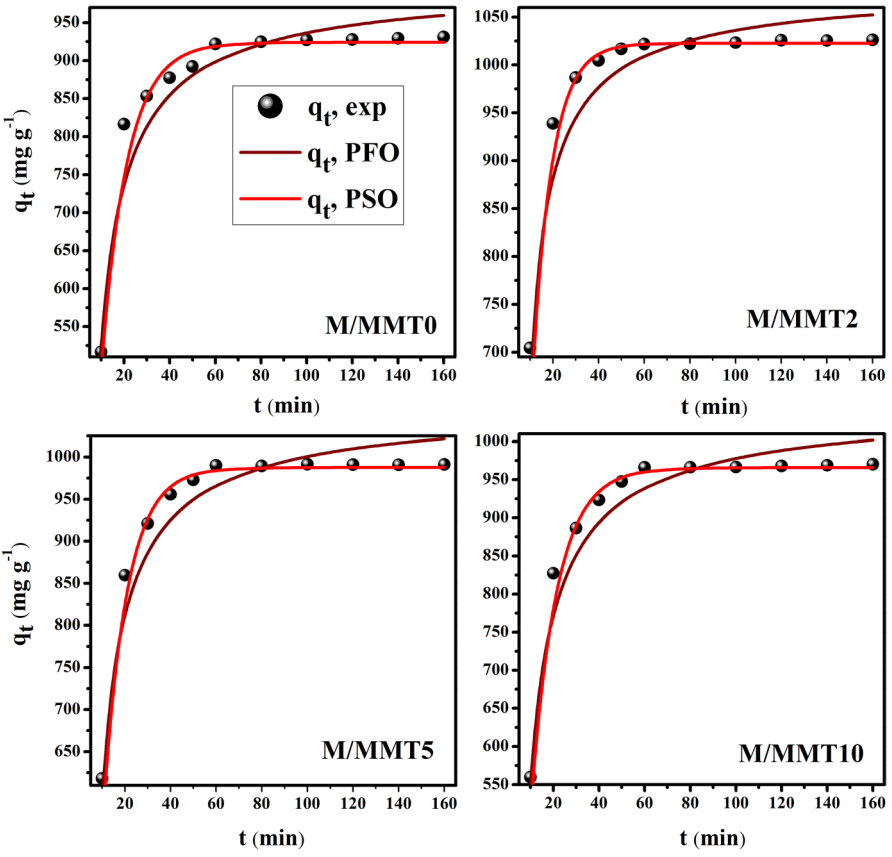

Fig. 9 Kinetics study of BR46 adsorption onto hydrogel matrix and its nanocomposites according to pseudo-first-order and pseudo-second-order kinetics models

Table 1 Nonlinear PFO and PSO kinetic parameters for the BR46 dye adsorption onto hydrogel matrix and its nanocomposites

Kinetic parameters	M/MMT**0**	M/MMT**2**	M/MMT**5**	M/MMT**10**
q_e exp (mg g^{-1})[a]	931.10	1026.2	991.4	970.2
Pseudo-first-order				
q_{e1} cal (mg g^{-1})	999.74	1079.6	1057.5	1042.6
k_1 (10^{-2} min^{-1})	8.89	11.82	9.81	8.88
R^2	0.990	0.995	0.995	0.993
SSE	155.41	98.58	94.45	120.32
Pseudo-second-order				
q_{e2} cal (mg g^{-1})	924.18	1022.6	987.48	965.68
k_2 (10^{-2} g mg^{-1} min^{-1})	0.049	0.022	0.017	0.015
R^2	0.998	0.999	0.999	0.999
SSE	41.08	3.37	6.20	11.77
Intra-particle diffusion				
First stage[b]				
$k_{id,1}$ (mg g^{-1} $min^{-0.5}$)	228.8	178.9	184.4	204.2
Second stage[b]				
$k_{id,2}$ (mg g^{-1} $min^{-0.5}$)	30.80	24.67	39.01	42.10
Third stage[b]				
$k_{id,3}$ (mg g^{-1} $min^{-0.5}$)	1.73	1.01	0.32	0.85

[a] $C_0 = 200$ mg L^{-1}, adsorbent dose = 0.1 g L^{-1}, T = 25 °C, pH 7; [b] $R^2 \geq 0.977$

Besides, the intra-particle diffusion kinetics model is defined by following Eq. (10).

$$q_t = k_{id} \cdot t^{0.5} + c \tag{10}$$

where k_{id} is the rate constant of intra-particle diffusion relation (mg g^{-1} $min^{-0.5}$) and C value indicates the thickness of boundary layer.

According to the equation, a plot of q_t versus $t^{0.5}$ should be a straight line and passes through origin when the adsorption mechanism follows intra-particle diffusion process that is the rate-limiting step; otherwise, more steps occur in the adsorption process.

It can be seen from Fig. 10 that the plotting exhibits three different straight lines for each dye-adsorbent system, indicating that dye adsorption onto MMT-free hydrogel and its nanocomposites is controlled not only by intra-particle diffusion. This result highlights three distinct stages in the sorption process for which the related rate constants (Table 1) are arranged in decreasing order as $k_{id,1} > k_{id,2} > k_{id,3}$. This behavior can be explained by the fact that initially (first sharper region), the process is controlled by rapid diffusion of BR46 molecules from bulk to the external surfaces of adsorbents due to the abundant and available active sites. The second stage is belonged to delay of dye molecules diffusion since the external active sites become unavailable, and then a slow intra-particle diffusion of dye molecules in

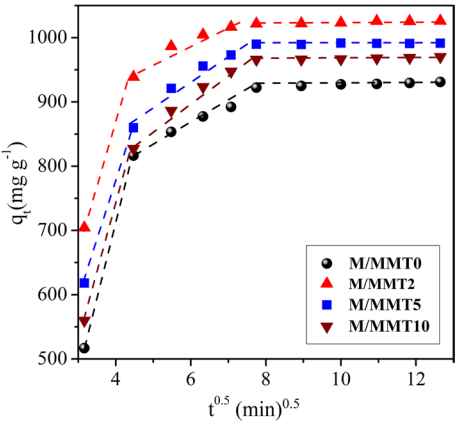

Fig. 10 Intra-particle diffusion model plots for the adsorption of BR46 onto free MMT hydrogel matrix and its nanocomposites composites

inner pores could be the limiting step. Lastly stage affirms equilibrium state reaching in where almost sites become saturated [36, 37, 61].

Adsorption isotherm models

Analysis of equilibrium data by isotherm models is very important to compare different sorbents under different operational conditions and to design and optimize an operating procedure. So, the most commonly Langmuir [62] and Freundlich [63] isotherm models were applied to describe the adsorbent–adsorbate interactions at equilibrium. Langmuir model assumes that a monolayer adsorption takes place on a homogeneous adsorbent surface. Contrariwise, Freundlich model postulates that a multilayer adsorption occurs by a heterogeneous adsorbent surface.

The nonlinear forms of Langmuir and Freundlich models are described by following Eqs. (11) and (12), respectively.

$$q_e = \frac{q_m K_L C_e}{\left(1 + K_L C_e\right)} \tag{11}$$

$$q_e = K_F \, C_e^{1/n} \tag{12}$$

where C_e is the residual equilibrium concentration of BR46 dye (mg L^{-1}), q_e is the dye amount at equilibrium (mg g^{-1}), K_L (L mg^{-1}) is Langmuir constant, and q_m is the Langmuir maximum equilibrium adsorption capacity (mg g^{-1}). K_F ((mg.g^{-1}) (L.mg^{-1})$^{(1/n)}$) is Freundlich constant, and 1/n is heterogeneity factor (more heterogeneous if 1/*n* gets close to zero and $(1/n) < 1$ or > 1 indicates an adsorption process chemically or physically driven, respectively).

Furthermore, the equilibrium dimensionless parameter R_L was calculated from Langmuir model to determine whether the adsorption process is favorable or not using following equation Eq. (13).

$$R_L = \frac{1}{1 + K_L C_0} \tag{13}$$

Depending on R_L value, the dye adsorption is favorable ($0 < R_L < 1$), unfavorable ($R_L > 1$), linear ($R_L = 1$), or irreversible ($R_L = 0$).

Langmuir and Freundlich nonlinear isotherm fitting using MATLAB 2013 program is shown in Fig. 11. The calculated parameters as well as the experimental equilibrium data and the error function SSE are regrouped in Table 2. It can be noticed that the R^2 values are upper for Langmuir model (0.994–0.987) than Freundlich model (0.974–0.957) and the calculated equilibrium capacities q_m from Langmuir model are close to experimental data. As well, the lowest SSE values are recorded for Langmuir model. These results confirm that Langmuir model is the best-fitting for the sequestration of BR46 dye onto homogeneous surfaces of hydrogel adsorbents through ideal monolayer coverage of dye onto binding sites and this process is not altered by the added MMT into nanohybrids. Moreover, the values

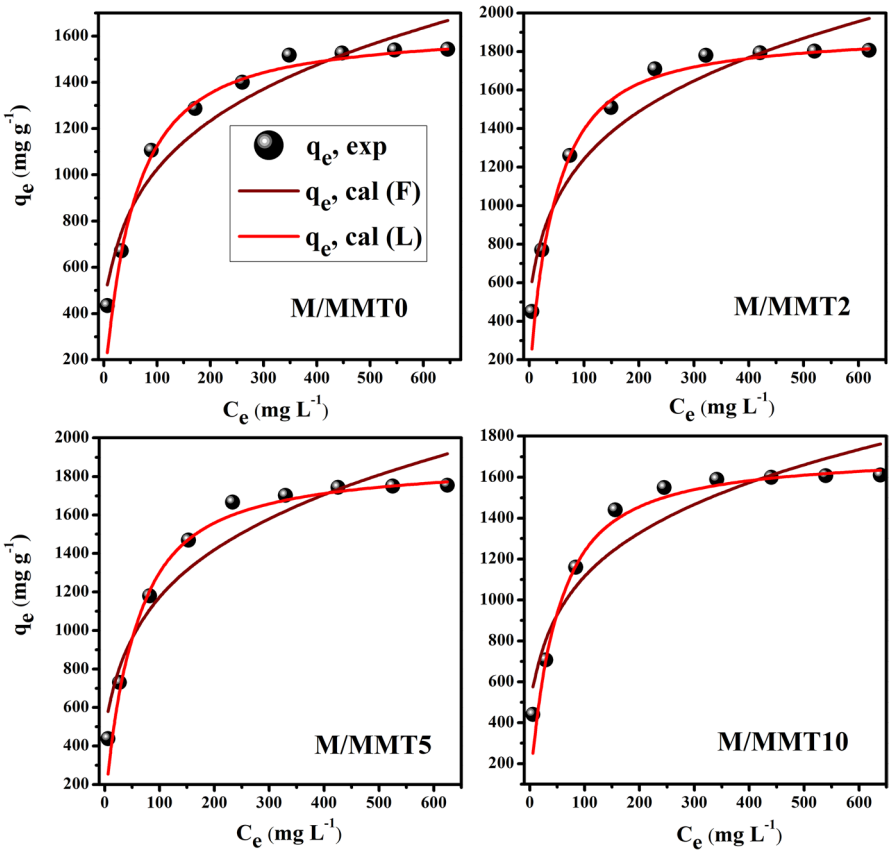

Fig. 11 Isotherm adsorption fitting according to nonlinear forms of Freundlich (F) and Langmuir (L) models

Table 2 Equilibrium isotherm parameters for the BR46 dye adsorption onto hydrogel matrix and its nanocomposites

Isotherm parameters	M/MMT**0**	M/MMT**2**	M/MMT**5**	M/MMT**10**
q_e exp (mg g^{-1})[a]	1543.3	1806.1	1754.3	1610.5
Langmuir model (L)				
q_m (mg g^{-1})	1553.2	1813.4	1763.3	1617.6
K_L (L mg^{-1})	0.02	0.03	0.02	0.03
R^2	0.987	0.991	0.994	0.988
SSE	51.82	51.71	47.37	50.68
R_L[b]	0.500	0.400	0.500	0.400
Freundlich model (F)				
K_F $(mg.g^{-1}).(L.mg^{-1})^{(1/n)}$	326.72	410.23	360.56	376.97
1/n	0.25	0.24	0.26	0.24
R^2	0.974	0.969	0.967	0.957
SSE	71.47	129.62	128.73	133.02

[a]Adsorbent 0.1 g L^{-1}, 25 °C, pH 7, 3 h; [b] calculated for lowest C_0 ($R_L < 0.1$ for higher C_0)

of R_L less than unity (0.4–0.5) imply favorable interactions of BR46 dye with M/MMT**x** hydrogels and those of 1/n below unity are indicative of chemisorption process. Analogs deductions have also been reported for hydrogels comprising inorganic additives [43–47].

As expected, the M/MMT**x** nanocomposites display the higher q_m values as compared to MMT-free hydrogel matrix. The obtained q_m values are 1553, 1813, and 1763 and 1617 mg g^{-1} for M/MMT**0**, M/MMT**2**, M/MMT**5**, and M/MMT**10** respectively.

For comparison, Table 3 regroups equilibrium maximum adsorption capacities q_m of M/MMT**x** hydrogel nanocomposites together with those of other adsorbents reported for their adsorption performances for BR46 dye [64–70]. For instance, dead *Pleurotus mutilus* as fungal biomass waste was used in BR46 removal from single and binary systems, where single sorption gives the maximum capacity equal

Table 3 Comparison of maximum equilibrium adsorption capacity for BR 46 dye onto different adsorbents reservoir

Adsorbents	q_m (mg g^{-1})	References
Dead *Pleurotus mutilus* biomass	76.92	[64]
Activated carbon from wild olive cores (oleaster)	781	[65]
As-grown and modified multi-walled carbon nanotubes	19 and 51	[66]
Activated Algerian clay	175	[67]
animal bone meal	24	[68]
rough and treated Algerian phosphates	28	[69]
Poly(acrylonitrile-co-pyrrole)/ZrO_2 NPs composites	500	[70]
Chitosan-g-polyacrylamide/MMT**x** hydrogel nanocomposites	1553–1813[a]	This study

[a]q_m values range of nanocomposites prepared by varying MMT content (x = 0, 2, 5, 10 wt.%)

to 76.92 mg g^{-1} [64]. Adsorption onto activated carbon from the wild olive cores an agricultural by-product is also significant being 781 mg g^{-1} [65], while lesser capacities values about 19 and 51 mg g^{-1} were obtained when using as-grown and modified multi-walled carbon nanotubes, respectively [66]. Among numerous inorganic materials, the activated clay has successfully adsorbed BR46 in monolayer with maximum capacity of 175 mg g^{-1} [67]. Calcinated animal bone meal [68], comprised of hydroxyapatite and carbonated fluorapatite type B with a specific surface area of 85 m^2/g, was also used as low-cost adsorbent with maximum capacity of 24 mg g^{-1}. Graba et al. [69] have reported on rough and treated phosphates and proved that chemical and thermal treatments affected negatively their adsorption capacity, leading to maximum value of 28.5 mg g^{-1}. In the case of hybrid organic/inorganic materials, nanopolymeric composite of poly(acrylonitrile-*co*-pyrrole) and zirconia nanoparticles has proved to be efficient for BR46 sequestration with q_m value of 500 mg g^{-1} [70]. It appears obvious that our hydrogels display excellent q_m capacities (up to 1813 mg g^{-1}) as compared to the above-cited materials. Thus, the developed M/MMT**x** hydrogel nanocomposites could be considered suitable adsorbents for efficient recovery of cationic dyes from contaminated water.

Thermodynamic parameters of adsorption and proposed mechanism

To further evaluate the influence of temperature variation on the BR46 dye adsorption and to inspect the nature of the process, the thermodynamic parameters [71] including Gibbs free energy change (ΔG°), standard entropy change (ΔS°), and standard enthalpy change (ΔH°) were assessed from the experimental data using Eqs. (14) and (15).

$$\Delta G^0 = -RT\,\mathrm{Ln}K_d \tag{14}$$

$$\mathrm{Ln}K_d = \frac{\Delta S^0}{R} - \frac{\Delta H^0}{RT} \tag{15}$$

where K_d is the distribution coefficient (dimensionless) obtained at equilibrium state by dividing the amount of BR46 dye adsorbed on the hydrogel sample (q_e) to the dye remaining in solution (C_e), R is the gas constant (8.314 J mol^{-1} K^{-1}), and T is the absolute temperature (K).

ΔH° and ΔS° values are obtained from the linear plot of ln K_d versus (1/T) (figure not shown).

Table 4 regroups the obtained thermodynamic parameters. As it can be seen, the negative values of ΔG° and their decrease with increasing temperature from 25 to 45 °C indicate that the adsorption is spontaneous and being thermodynamically more favorable at higher temperatures. The positive value of ΔH^0 confirms the endothermic nature of the process. In addition, the magnitude of ΔH° depends on the type of interactions involved in the adsorption process, where ΔH° value found in the range from 2 to 40 kJ mol^{-1} is ascribed to van der Waals forces, dipole bond forces, hydrogen bonding, and/or coordination exchange [44, 53, 56]. Therefore, the obtained ΔH° value suggests the occurrence of physisorption via most

Table 4 Thermodynamic parameters for BR46 adsorption onto hydrogel adsorbents M/MMT**x**

Adsorbent	$\Delta G°$ (kJ mol^{-1}) at T(K)			ΔH^0 (kJ mol^{-1})	ΔS^0 (J mol^{-1} K^{-1})
	298	308	318		
M/MMT**0**	−4.201	−4.635	−5.140	21.657	39.167
M/MMT**2**	−4.747	−5.161	−5.796	20.854	43.557
M/MMT**5**	−4.544	−4.911	−5.499	20.350	39.342
M/MMT**10**	−4.273	−4.660	−5.224	19.365	39.541

likely electrostatic interactions as well as hydrogen bonding. The positive ΔS^0 value reflects good affinity of dye toward the sorbents and increased randomness at the solid-solution interface during the fixation of the BR46 dye on the active sites of the hydrogel nanocomposites.

Based on the aforementioned results, it can be clearly speculate that the plausible adsorption mechanism may be due to some noncovalent interactions, namely electrostatic interactions and hydrogen bonding, which can contribute to the adsorption when they act synergistically and the process becomes much stronger than that driven by the same interactions acting individually.

A conceptual illustration of interactions between nanocomposites and BR46 dye during adsorption process is given in Fig. 12. Accordingly, two mechanisms of adsorption may occur: The main one is driven from ionic interactions of the active binding groups of absorbents, namely the carboxylate groups of crosslinked PAAm

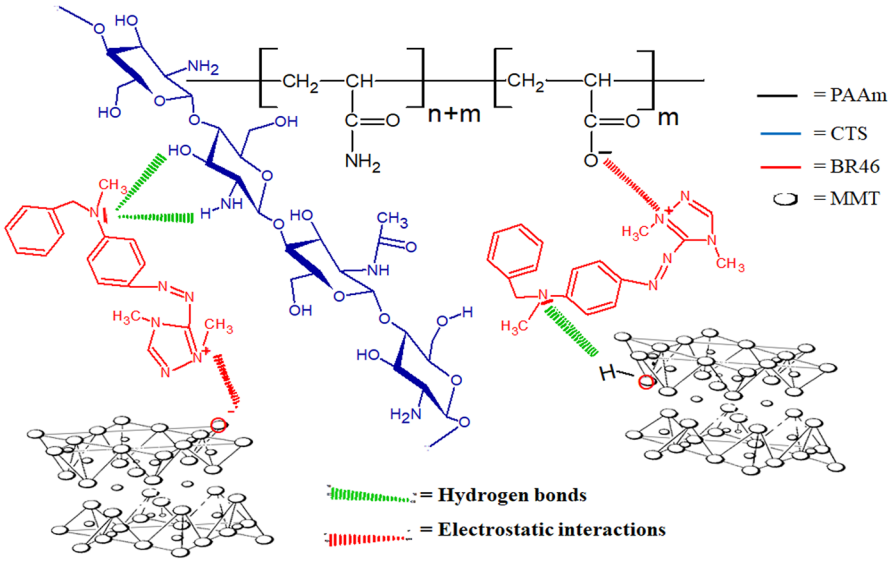

Fig. 12 Schematic illustrations of interactions between the M/MMT**x** hydrogel nanocomposites and the BR46 dye during adsorption process

chains and the negatively charges of MMT surface layers, with the quaternary ammoniums of BR46 molecules. In the second one, the –OH hydroxyls groups of the MMT surfaces and/or CTS chains could be implicated in the removal of dye through hydrogen bonding interactions developed with the amino groups of dye.

Desorption and regeneration study

The regeneration of adsorbents is an important economic process for the large-scale effluent treatment since the industrial applicability of an effective adsorbent is additionally subject to the recovery ability. Therefore, the reusability of the optimized M/MMT**2** hydrogel nanohybrid and the MMT-free matrix was assessed in four adsorption/desorption cycles.

From the results presented in Fig. 13, it is noted that desorption percentage is greater than 91% for all cycles, indicating effectiveness of the desorbing agent. In addition, the removal efficiencies slight decrease with increasing cycle time and remain about 86% and 83.6% after 4th cycle for M/MMT**0** and M/MMT**2**, respectively. The results reveal that these hydrogel adsorbents are recyclable and can be reused in next batches for the discoloration of polluted water, which will reduce the cost of process.

Conclusion

In the current study, we have successfully elaborated porous hydrolyzed CTS-graft-PAAm/MMT**x** hydrogels nanocomposites, characterized, and then systematically inspected in adsorptive removal of Basic Red 46 dye under different adsorption conditions. The results have revealed that the incorporation of a small amount of MMT into the grafted matrix as well as the use of Triton X-100 surfactant as the pore-forming agent contributed to improve the porous structure, swelling capacity

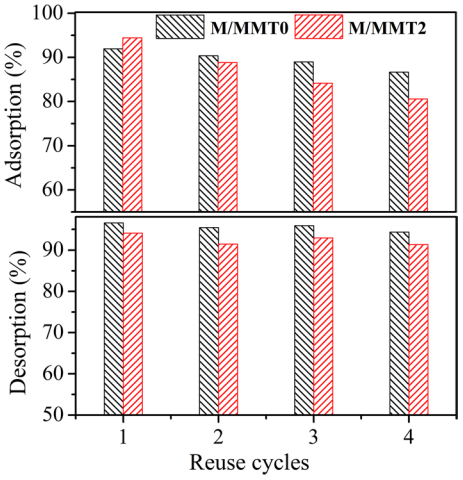

Fig. 13 Reusability results of hydrogel matrix and its nanocomposite in four adsorption/desorption cycles for BR 46 dye (0.1 g L^{-1} of adsorbent, C_0 of 200 mg L^{-1}, 3 h, pH 7, 25 °C)

of the resulting nanocomposites. The results of dye adsorption on these hydrogels confirmed that contact time, temperature, pH, initial dye concentration, and hydrogel dose affected effectively the dye removal. The experimental data were correlated with pseudo-second-order kinetic model, whereas the intra-particle diffusion was not the only rate-controlling step. The isotherm data were well fitted by Langmuir model, confirming physisorption mechanism. The calculated value of monolayer adsorption capacity (q_m) of hydrogel matrix was increased from 1550 mg g^{-1} to an optimum of 1813 mg g^{-1} by adding only 2 wt. % MMT. The thermodynamics study evidenced the spontaneity of the process and its endothermic nature. The adsorption–desorption process was observed to be effective in repeated cycles, indicating the reusability of the hydrogels for dye removal applications. Finally, the successful regeneration of these adsorbents could be practical for their use for removal of pollutants dyes from contaminated solutions with reduced costs at industrial scale.

References

1. Yusuf M, Shabbir M, Mohammad F (2017) Natural colorants: historical, processing and sustainable prospects. Nat Products Bioprospect 7:123
2. Lellis B, Fávaro-Polonio CZ, Pamphile JA, Polonio JC (2019) Effects of textile dyes on health and the environment and bioremediation potential of living organisms. Biotechnol Res Innov 3:275
3. Karim AB, Mounir B, Hachkar M, Bakasse M, Yaacoubi A (2009) Removal of basic red 46 dye from aqueous solution by adsorption onto moroccan clay. J Hazard Mater 168:304
4. Agueniou F, Chebli D, Reffas A, Bouguettoucha A, Benguerba Y, Favier L, Amrane A (2018) Impact of TiO_2–cation exchange resin composite on the removal of ethyl violet. Arab J Sci Eng 43:2451
5. Teh CY, Budiman PM, Shak KPY, Wu TY (2016) Recent advancement of coagulation-flocculation and its application in wastewater treatment. Ind Eng Chem Res 55:4363
6. Karisma D, Febrianto G, Mangindaan D (2018) Removal of dyes from textile wastewater by using nanofiltration polyetherimide membrane. IOP Conference Series: Earth and environmental science. Institute of Physics Publishing, p 12012
7. Katheresan V, Kansedo J, Lau SY (2018) Efficiency of various recent wastewater dye removal methods a review. J Environ Chem Eng 6:4676
8. Yagub MT, Sen TK, Afroze S, Ang HM (2014) Dye and its removal from aqueous solution by adsorption a review. Adv Colloid Interface Sci 209:172
9. Shabaan OA, Jahin HS, Mohamed GG (2020) Removal of anionic and cationic dyes from wastewater by adsorption using multiwall carbon nanotubes. Arab J Chem 13:4797
10. Jency M, Krishnaveni J (2020) Adsorptive removal of dyes onto cost effective biomaterials a review. J Environ Treat Tech 9:218
11. Abd-Elhamid AI, Emran M, El-Sadek MH, El-Shanshory AA, Soliman HMA, Akl MA, Rashad M (2020) Enhanced removal of cationic dye by eco-friendly activated biochar derived from rice straw. Appl Water Sci 10:45
12. Kausar A, Iqbal M, Javed A, Aftab K, Nazli ZIH, Bhatti HN, Nouren S (2018) Dyes adsorption using clay and modified clay a review. J Mol Liq 256:395
13. Maged A, Iqbal J, Kharbish S, Ismael IS, Bhatnagar A (2020) Tuning tetracycline removal from aqueous solution onto activated 2:1 layered clay mineral: characterization, sorption and mechanistic studies. J Hazard Mater 384:121320
14. Menya E, Olupot PW, Storz H, Lubwama M, Kiros Y (2018) Production and performance of activated carbon from rice husks for removal of natural organic matter from water a review. Chem Eng Res Des 129:271
15. Pan Y, Shi X, Cai P, Guo T, Tong Z, Xiao H (2018) Dye removal from single and binary systems using gel-like bioadsorbent based on functional-modified cellulose. Cellulose 25:2559

16. Kausar A, Shahzad R, Iqbal J, Muhammad N, Ibrahim SM, Iqbal M (2020) Development of new organic-inorganic, hybrid bionanocomposite from cellulose and clay for enhanced removal of drimarine yellow HF-3GL dye. Int J Biol Macromol 149:1059
17. Song Y, Tan J, Wang G, Zhou L (2018) Superior amine-rich gel adsorbent from peach gum polysaccharide for highly efficient removal of anionic dyes. Carbohydr Polym 199:178
18. Shariatinia Z, Jalali AM (2018) Chitosan-based hydrogels: preparation, properties and applications. Int J Biol Macromol 115:194
19. Tomadoni B, Salcedo MF, Mansilla AY, Casalongué CA, Alvarez VA (2020) Macroporous alginate-based hydrogels to control soil substrate moisture: effect on lettuce plants under drought stress. Eur Polym J 137:109953
20. Shalla AH, Bhat MA, Yaseen Z (2018) Hydrogels for removal of recalcitrant organic dyes: a conceptual overview. J Environ Chem Eng 6:5938
21. Farag AM, Sokker HH, Zayed EM, Nour Eldien FA, Abd Alrahman NM (2018) Removal of hazardous pollutants using bifunctional hydrogel obtained from modified starch by grafting copolymerization. Int J Biol Macromol 120:2188
22. Mittal H, Ray SS, Okamoto M (2016) Recent progress on the design and applications of polysaccharide-based graft copolymer hydrogels as adsorbents for wastewater purification. Macromol Mater Eng 301:496
23. Ferfera-Harrar H, Aouaz N, Dairi N (2016) Environmental sensitive chitosan-g-polyacrylamide/carboxymethylcellulose superabsorbent composites for wastewater purification I: synthesis and properties. Polym Bull 73:815
24. Sharma P, Borah DJ, Das P, Das MR (2016) Cationic and anionic dye removal from aqueous solution using montmorillonite clay: evaluation of adsorption parameters and mechanism. Desalin Water Treat 57:8372
25. Amari A, Gannouni H, Khan MI, Almesfer MK, Elkhaleefa AM, Gannouni A (2018) Effect of structure and chemical activation on the adsorption properties of green clay minerals for the removal of cationic dye. Appl Sci 8:2302
26. Wang Q, Wang Y, Chen L (2019) A green composite hydrogel based on cellulose and clay as efficient absorbent of colored organic effluent. Carbohydr Polym 210:314
27. Dominguez MA, Etcheverry M, Zanini GP (2019) Evaluation of the adsorption kinetics of brilliant green dye onto a montmorillonite/alginate composite beads by the shrinking core model. Adsorption 25:1387
28. Nagarpita MV, Roy P, Shruthi SB, Sailaja RRN (2017) Synthesis and swelling characteristics of chitosan and CMC grafted sodium acrylate-co-acrylamide using modified nanoclay and examining its efficacy for removal of dyes. Int J Biol Macromol 102:1226
29. Zhang L, Zeng Y, Cheng Z (2016) Removal of heavy metal ions using chitosan and modified chitosan a review. J Mol Liq 214:175
30. Mittal H, Al Alili A, Morajkar PP, Alhassan SM (2021) GO crosslinked hydrogel nanocomposites of chitosan/carboxymethyl cellulose – a versatile adsorbent for the treatment of dyes contaminated wastewater. Int J Biol Macromol 167:1248
31. Wang Y, Wang H, Peng H, Wang Z, Wu J, Liu Z (2018) Dye adsorption from aqueous solution by cellulose/chitosan composite: equilibrium, kinetics, and thermodynamics. Fibers Polym 19:340
32. Vaz MG, Pereira AGB, Fajardo AR, Azevedo ACN, Rodrigues FHA (2017) Methylene blue adsorption on chitosan-g-poly(acrylic acid)/rice husk ash superabsorbent composite: kinetics, equilibrium, and thermodynamics. Water Air Soil Pollut 228:1
33. Ferfera-Harrar H, Aiouaz N, Dairi N, Hadj-Hamou AS (2014) Preparation of chitosan-g-poly(acrylamide)/montmorillonite superabsorbent polymer composites: studies on swelling, thermal, and antibacterial properties. J Appl Polym Sci 131:39747
34. Wei Q (2014) Fast-swelling porous starch-g-poly(acrylic acid) superabsorbents. Iran Polym J 23:637
35. Benhalima T, Ferfera-Harrar H, Lerari D (2017) Optimization of carboxymethyl cellulose hydrogels beads generated by an anionic surfactant micelle templating for cationic dye uptake: swelling, sorption and reusability studies. Int J Biol Macromol 105:1025
36. Benhalima T, Ferfera-Harrar H (2019) Eco-friendly porous carboxymethyl cellulose/dextran sulfate composite beads as reusable and efficient adsorbents of cationic dye methylene blue. Int J Biol Macromol 132:126
37. Ferfera-Harrar H, Dairi N (2013) Elaboration of cellulose acetate nanobiocomposites using acidified gelatin-montmorillonite as nanofiller: morphology, properties, and biodegradation studies. Polym Compos 34:1515

38. Zhang J, Wang L, Wang A (2007) Preparation and properties of chitosan-g-poly(acrylic acid)/montmorillonite superabsorbent nanocomposite via in situ intercalative polymerization. Ind Eng Chem Res 46:2497
39. Liu J, Wang A (2008) Study on superabsorbent composites. XXI. Synthesis, characterization and swelling behaviors of chitosan-g-poly(acrylic acid)/organo-rectorite nanocomposite superabsorbents. J Appl Polym Sci 110:678
40. Darder M, Colilla M, Ruiz-Hitzky E (2005) Chitosan-clay nanocomposites: application as electrochemical sensors. Appl Clay Sci 28:199
41. Bao Y, Ma J, Li N (2011) Synthesis and swelling behaviors of sodium carboxymethyl cellulose-g-poly(AA-co-AM-co-AMPS)/MMT superabsorbent hydrogel. Carbohyd Polym 84:76
42. Zhang J, Wang Q, Wang A (2007) Synthesis and characterization of chitosan-g-poly(acrylicacid)/attapulgite superabsorbent composites. Carbohyd Polym 68:367
43. Hosseinzadeh H, Zoroufi S, Mahdavinia GR (2015) Study on adsorption of cationic dye on novel kappa-carrageenan/poly(vinyl alcohol)/montmorillonite nanocomposite hydrogels. Polym Bull 72:1339
44. Liu C, Omer AM, Ouyang XK (2018) Adsorptive removal of cationic methylene blue dye using carboxymethyl cellulose/k-carrageenan/activated montmorillonite composite beads: isotherm and kinetic studies. Int J Biol Macromol 106:823
45. Wang L, Zhang J, Wang A (2008) Removal of methylene blue from aqueous solution using chitosan-g-poly(acrylic acid)/montmorillonite superadsorbent nanocomposite. Colloids Surf A Physicochem Eng Asp 322:47
46. Wang L, Zhang J, Wang A (2011) Fast removal of methylene blue from aqueous solution by adsorption onto chitosan-g-poly(acrylic acid)/attapulgite composite. Desalination 266:33
47. Liu Y, Zheng Y, Wang A (2010) Enhanced adsorption of methylene blue from aqueous solution by chitosan-g-poly (acrylic acid)/vermiculite hydrogel composites. J Environ Sci 22:486
48. Cai T, Yang Z, Li H, Yang H, Li A, Cheng R (2013) Effect of hydrolysis degree of hydrolyzed polyacrylamide grafted carboxymethyl cellulose on dye removal efficiency. Cellulose 20:2605
49. Parlayici Ş (2019) Alginate-coated perlite beads for the efficient removal of methylene blue, malachite green, and methyl violet from aqueous solutions: kinetic, thermodynamic, and equilibrium studies. J Anal Sci Technol 10:4
50. Tan J, Xie S, Wang G, Yu CW, Zeng T, Cai P, Huang H (2020) Fabrication and optimization of the thermo-sensitive hydrogel carboxymethyl cellulose/poly(n-isopropylacrylamide-co-acrylic acid) for U(VI) removal from aqueous solution. Polymers (Basel) 12:151
51. Eltaweil AS, Elgarhy GS, El-Subruiti GM, Omer AM (2020) Carboxymethyl cellulose/carboxylated graphene oxide composite microbeads for efficient adsorption of cationic methylene blue dye. Int J Biol Macromol 154:307
52. Asadi S, Eris S, Azizian S (2018) Alginate-based hydrogel beads as a biocompatible and efficient adsorbent for dye removal from aqueous solutions. ACS Omega 3:15140
53. Thakur S, Pandey S, Arotiba OA (2016) Development of a sodium alginate-based organic/inorganic superabsorbent composite hydrogel for adsorption of methylene blue. Carbohydr Polym 153:34
54. Duman O, Polat TG, Diker CÖ, Tunç S (2020) Agar/κ-carrageenan composite hydrogel adsorbent for the removal of methylene blue from water. Int J Biol Macromol 160:823
55. Gerente C, Lee VKC, Le Cloirec P, McKay G (2007) Application of chitosan for the removal of metals from wastewaters by adsorption - mechanisms and models review. Crit Rev Environ Sci Technol 37:41
56. Moussout H, Ahlafi H, Aazza M, Maghat H (2018) Critical of linear and nonlinear equations of pseudo-first order and pseudo-second order kinetic models. Karbala Int J Mod Sci 4:244
57. Ho YS (2006) Second-order kinetic model for the sorption of cadmium onto tree fern: a comparison of linear and non-linear methods. Water Res 40:119
58. Weber W, Morris JC (1963) Kinetics of adsorption on carbon from solution. J Sanit Eng Div Proc Am Soc Eng 89:31
59. Kausar A, Naeem K, Tariq M, Nazli ZIH, Bhatti HN, Jubeen F, Nazir A, Iqbal M (2019) Preparation and characterization of chitosan/clay composite for direct rose FRN dye removal from aqueous media: comparison of linear and non-linear regression methods. J Mater Res Technol 8:1161
60. Zamouche M, Habib A, Saaidia K, Bencheikh Lehocine M (2020) Batch mode for adsorption of crystal violet by cedar cone forest waste. SN Appl Sci 2:1

61. Bhatti HN, Safa Y, Yakout SM, Shair OH, Iqbal M, Nazir A (2020) Efficient removal of dyes using carboxymethyl cellulose/alginate/polyvinyl alcohol/rice husk composite: adsorption/desorption, kinetics and recycling studies. Int J Biol Macromol 150:861
62. Langmuir I (1916) The constitution and fundamental properties of solids and liquids. Part I. Solids. J Am Chem Soc 38:2221
63. Freundlich HMF (1906) Over the adsorption in solution. J Phys Chem 57:1100
64. Yeddou Mezenner N, Hamadi A, Kaddour S, Bensaadi Z, Bensmaili A (2013) Biosorption behavior of basic red 46 and violet 3 by dead pleurotus mutilus from single- and multicomponent systems. J Chem 2013:1
65. Kaouah F, Boumaza S, Berrama T, Trari M, Bendjama Z (2013) Preparation and characterization of activated carbon from wild olive cores (oleaster) by H_3PO_4 for the removal of basic red 46. J Clean Prod 54:296
66. Konicki W, Pełech I (2019) Removing cationic dye from aqueous solutions using as-grown and modified multi-walled carbon nanotubes. Polish J Environ Stud 28:717
67. Elhadj M, Samira A, Mohamed T, Djawad F, Asma A, Djamel N (2020) Removal of basic red 46 dye from aqueous solution by adsorption and photocatalysis: equilibrium, isotherms, kinetics, and thermodynamic studies. Sep Sci Technol 55:867
68. El Haddad M, Mamouni R, Saffaj N, Lazar S (2012) Removal of a cationic dye - basic red 12 - from aqueous solution by adsorption onto animal bone meal. J Assoc Arab Univ Basic Appl Sci 12:48
69. Graba Z, Hamoudi S, Bekka D, Bezzi N, Boukherroub R (2015) Influence of adsorption parameters of basic red dye 46 by the rough and treated Algerian natural phosphates. J Ind Eng Chem 25:229
70. El-Kady MF, El-Aassar MR, El Batrawy OA, Ibrahim MS, Hassan HS, Fakhry H (2018) Equilibrium and kinetic behaviors of cationic dye decolorization using poly(AN-co-Py)/ZrO_2 novel nanopolymeric composites. Adv Polym Technol 37:740
71. Lima EC, Hosseini-Bandegharaei A, Moreno-Piraján JC, Anastopoulos I (2019) A critical review of the estimation of the thermodynamic parameters on adsorption equilibria. Wrong use of equilibrium constant in the Van't Hoof equation for calculation of thermodynamic parameters of adsorption. J Mol Liq 273:425

Authors and Affiliations

Hafida Ferfera-Harrar[1] · Tayeb Benhalima[1,2] · Amina Sadi[1]

✉ Hafida Ferfera-Harrar
harrarhafida@yahoo.fr

[1] Materials Polymer Laboratory, Macromolecular Chemistry Department, Faculty of Chemistry, University of Sciences and Technology Houari Boumediene (USTHB), B.P. 32 El-Alia, 16111 Algiers, Algeria

[2] Unité de Recherche en Analyses Et Développement Technologiques en Environnement-Centre de Recherche Scientifique Et Technique en Analyses Physico-Chimiques UR-ADTE- CRAPC, BP 384, Tipaza, Algeria